

# Author's Accepted Manuscript

Fracture in Annealed and Severely Deformed Tungsten

Zachary S. Levin, Ankit Srivastava, David C. Foley, Karl T. Hartwig



PII: S0921-5093(18)30644-0  
DOI: <https://doi.org/10.1016/j.msea.2018.05.004>  
Reference: MSA36442

To appear in: *Materials Science & Engineering A*

Received date: 7 December 2017  
Revised date: 1 May 2018  
Accepted date: 2 May 2018

Cite this article as: Zachary S. Levin, Ankit Srivastava, David C. Foley and Karl T. Hartwig, Fracture in Annealed and Severely Deformed Tungsten, *Materials Science & Engineering A*, <https://doi.org/10.1016/j.msea.2018.05.004>

This is a PDF file of an unedited manuscript that has been accepted for publication. As a service to our customers we are providing this early version of the manuscript. The manuscript will undergo copyediting, typesetting, and review of the resulting galley proof before it is published in its final citable form. Please note that during the production process errors may be discovered which could affect the content, and all legal disclaimers that apply to the journal pertain.

## Fracture in Annealed and Severely Deformed Tungsten

Zachary S. Levin<sup>1</sup>, Ankit Srivastava<sup>2</sup>, David C. Foley<sup>3</sup>, and Karl T. Hartwig<sup>2</sup>

<sup>1</sup>Airforce Research Laboratory, Kirtland AFB, NM 87117

<sup>2</sup>Department of Materials Science and Engineering, Texas A&M University College Station, TX 77843-3003, USA

<sup>3</sup>Shear Form, Inc. 207 Dellwood St. Bryan, TX 77801, USA

### Abstract

Bulk tungsten normally undergoes brittle fracture at ambient temperatures and has a brittle-to-ductile transition in the range 200-300°C. This limits the use of tungsten for a host of applications. In general, the fracture mode of tungsten at ambient temperature is intergranular whereas at high temperatures it undergoes transgranular fracture. In this work the focus is on the influences of microstructure and temperature on three-point bend fracture of polycrystalline pure tungsten. The samples were processed by equal channel angular extrusion (ECAE) through a 90° die angle via route A in order to produce an elongated microstructure. The mechanical behavior of both unprocessed and processed materials were then characterized by three-point bending at temperatures ranging from -45°C to 425°C. The results show that a single ECAE extrusion (strain ~1.15) reduces the flexural toughness of the material and increases the brittle-to-ductile transition temperature, while two and four extrusions dramatically increase the flexural toughness with little effect on the transition temperature compared to that of the unprocessed material. The flexural toughness of the material subjected to four extrusions (strains exceeding 4.5) is more than 50 times greater than that of the unprocessed material at ambient temperature. This is mainly due to microstructural changes that increases the resistance to intergranular fracture, enhances plastic dissipation, and activates relatively high fracture toughness crack systems for transgranular fracture. The results show that substantial elongation of grains by deformation processing at a temperature near the brittle-to-ductile transition temperature is an effective method for improving the ambient temperature ductility and toughness of bulk polycrystalline tungsten.

**Keywords:** Brittle-to-ductile transition; Failure Analysis; Fracture; Tungsten; Equal channel angular extrusion; ECAP.

### 1. Introduction

At ambient temperatures tungsten undergoes brittle fracture with no appreciable ductility. This brittle nature poses a significant hurdle for many applications which would benefit from its other attractive properties such as, high density (~19.3 g/cm<sup>3</sup>), high melting temperature (~3422°C), and high strength (~3GPa). The unfortunate poor ductility of tungsten is due to two factors: a low intergranular fracture energy [1, 2], and a relatively high ductile-to-brittle (with decreasing temperature) or brittle-to-ductile (with increasing temperature) transition temperature, generally accepted to be in the range of 200-300°C. The brittle-to-ductile transition temperature of tungsten is affected by impurities, strain rate, surface finish, and microstructural features including dislocation density, grain morphology, and texture [3].

In commercially available bulk tungsten, fracture occurs primarily through the separation of the tungsten grains. This mode of failure, referred to as intergranular fracture, is caused by poor cohesion between adjacent tungsten grains and has been shown to influence the mechanical behavior of polycrystalline tungsten [4-6]. The intergranular fracture is exacerbated by the affinity of the grain boundary region for interstitial impurities, due in part to the high grain boundary energy of tungsten. These interstitial species, primarily oxygen and carbon, at the grain boundaries impede dislocation mobility across grains further weakening the intergranular cohesion. Interstitial impurities that preferentially inhabit the grain boundaries can weaken these boundaries even at low concentration, resulting in brittle behavior [7-10]. The morphology of the grains in polycrystalline tungsten affects the extent of crack deflection. This can cause a shift from predominantly opening mode of crack growth to a mixed mode of opening and sliding of cracks [11, 12]. Under certain conditions, transgranular fracture, cracks propagating through the grain, is also observed. Transgranular fracture in general results in the opening mode of crack growth [11]. Improved fracture resistance in polycrystalline tungsten appears possible by reducing grain boundary impurities, altering grain morphology, and inducing appropriate metallographic texture.

Heavily worked wire/filament or sheet tungsten that possess a highly refined fibrous microstructure with a significant {110} texture along the fiber direction does exhibit significant ductility and substantial resistance to fracture at ambient temperatures [1, 13-15]. However, the improvement in the mechanical behavior is observed in the as-worked state only and recrystallization causes a dramatic decrease in ductility [1]. This suggests that bulk tungsten with a wire or sheet like microstructure may exhibit similar ambient temperature fracture resistance and ductility. Producing this microstructure in bulk material is not easy by conventional powder metallurgy and the commercial techniques used to fabricate small diameter tungsten wire. The conventional process involves, sintering, swaging, area reduction extrusion, and wire drawing (at progressively decreasing temperatures). An impractically large starting size would be required in order to follow the same area reduction steps to produce end product sizes for structural and other bulk applications.

Equal channel angular extrusion (ECAE), which can impart large plastic strains and give microstructure elongation without the area reduction of conventional processing is a viable alternative [16]. In a recent work, we carried out ECAE processing of commercially pure polycrystalline tungsten [17]. The as-received material was successfully processed to strains exceeding 4.5 at a low homologous temperature by multi-pass ECAE. It was shown that it is possible to develop a lamellar microstructure in bulk tungsten by this method with strong {110} and {111} texture along the extrusion direction similar to that of a drawn tungsten wire. In [17], the mechanical properties of the ECAE processed materials were also characterized by three-point bending. The ambient temperature flexural strength and the total flexural strain to failure of the material, ECAE processed to strains exceeding 4.5, was found to be greater than 3GPa, and ~20%, respectively.

The current work examines the influence of microstructure and temperature on three-point bend fracture of polycrystalline tungsten. The brittle-to-ductile transition and fracture mechanisms of unprocessed (as-received) and ECAE processed tungsten through a 90° die angle via route A are characterized in the temperature range, -45°C to 425°C. The results show that a single ECAE

extrusion reduces the flexural toughness of the as-received material and may increase the brittle-to-ductile transition temperature by a small amount. Additional extrusions increase the toughness of the material and return the transition temperature to, at or below, that of the as-received material. The flexural toughness of the material subjected to four extrusions is nearly two orders of magnitude greater than that of the as-received material at ambient temperatures. At ambient temperatures the as-received material fails predominantly by intergranular fracture whereas at high temperatures the fracture mode is transgranular. The material subjected to four extrusions failed by continuous intergranular separation and transgranular fracture at all test temperatures. It is noteworthy that this investigation is the first that we know of to examine the brittle-to-ductile transition and fracture mechanisms in heavily cold worked bulk polycrystalline tungsten.

## 2. Material description and experimental procedure

Rods of commercially pure (~99.97%) tungsten of diameter 12.7mm were obtained from Plansee Corp. (Reutte Austria). The rods were encapsulated snugly inside 25.4mm square 304 stainless steel cans and sealed by welding with argon cover gas.

Equal channel angular extrusions were carried out using a 25.4mm square 90° die angle sliding wall tool with temperature control. The encapsulated tungsten/stainless steel composite billets were lubricated and placed in the ECAE tool at ~300°C for one hour prior to extrusion to insure temperature equilibrium. Billets were extruded at a rate less than 1mm/s. Following extrusion, billets were machined to remove flash and resize for reinsertion into the die/tool. Billets were not rotated between extrusions, a strategy generally referred to as “route A” ECAE processing. This multi-pass approach is referred to as route, A, processing. Billets were subjected to a maximum of four isothermal extrusions at ~300°C. Post extrusion, the billets were quickly removed from the tool, and cooled in ambient air to ambient temperature. Hereafter, the ECAE processed material is designated based on the ECAE route and number of passes: 1A, 2A and 4A, where the number preceding the letter, A, (denoting ECAE route A) denotes the number of ECAE passes. The unprocessed material is designated, as-received or simply AR.

Three-point bend specimens of dimensions  $1 \times 2 \times 14 \text{ mm}^3$  with their length oriented along the extrusion direction (for ECAE processed materials) were machined using electrical discharge machining (EDM). The specimens were mechanically ground to remove the EDM surface effects and then electro-polished using an aqueous 1% NaOH solution. Bend test experiments were conducted using a custom apparatus with a bottom support span of 7mm. The upper and lower fixtures were made from H13 tool steel heat treated to a hardness of over 50HRC. Precision ground 0.2mm diameter tungsten carbide (WC) rods were used as sample support and loading pins for this apparatus. These pins, two bottom and one top, were placed into cylindrical sockets in the test apparatus, and secured with nickel wire. Before insertion of pins, both the sockets and WC rods were coated with graphite to reduce friction. The broad  $2 \times 14 \text{ mm}^2$  face of the test specimens was placed on the bottom supports so that the material (billet) top (longitudinal) plane was normal to the applied load. Samples were tested under displacement-controlled conditions at a rate less than 0.1mm/s. The testing temperature was controlled by use of a clamshell type furnace, which was calibrated with a surrogate specimen instrumented with a K-type thermocouple. This instrumented specimen was placed in the test apparatus at the same cross

head starting position used during testing. The furnace temperature was then calibrated using this instrumented sample and a nickel clad K-type thermocouple placed inside the furnace at the intended test specimen location. At elevated temperatures argon was used as a protective gas to suppress tungsten oxidation. Testing below ambient temperature was done by exposing the sample to refrigerant that undergoes a liquid-to-gas phase change at  $-45^{\circ}\text{C}$ . This temperature was measured directly with an instrumented specimen.

Post deformation, three-point bend specimens were examined through optical and electron microscopy. Electron microscopy was carried out using a FEI Quanta 600 FE-SEM scanning electron microscope (SEM) equipped with secondary electron (SE) and backscatter electron (BSE) detectors.

### 3. Experimental results

In a recent work on the same ECAE processed materials published previously [17], we showed that it is possible to develop a lamellar microstructure in bulk tungsten with strong  $\{110\}$  and  $\{111\}$  texture along the ECAE extrusion direction, which is similar to that of a drawn tungsten wire. The representative microstructures of the as-received and 4A materials are shown in Fig. 1. The as-received material contains nearly equiaxed grains. During ECAE processing, significant breakup and refinement of the microstructure takes place, and after four ECAE passes the grains become refined, elongated, and textured. In [17], the mechanical properties of the as-received and ECAE processed (1A, 2A and 4A) materials were characterized using Vickers hardness measurements and three-point bend tests. The Vickers hardness of the as-received and ECAE processed tungsten was found to exhibit a Hall-Petch type relationship with the average subgrain size. In addition, at ambient temperature the flexural strength of the 4A material was found to be greater than 3GPa and the total flexural strain to failure  $\sim 20\%$ . In the current work we focus on the brittle-to-ductile transition and failure characteristics of the as-received and ECAE processed materials at temperatures ranging from  $-45^{\circ}\text{C}$  to  $425^{\circ}\text{C}$ . The focus in this manuscript is the as-received and 4A materials, but for the sake of completeness, some results pertaining to 1A and 2A materials are also presented.

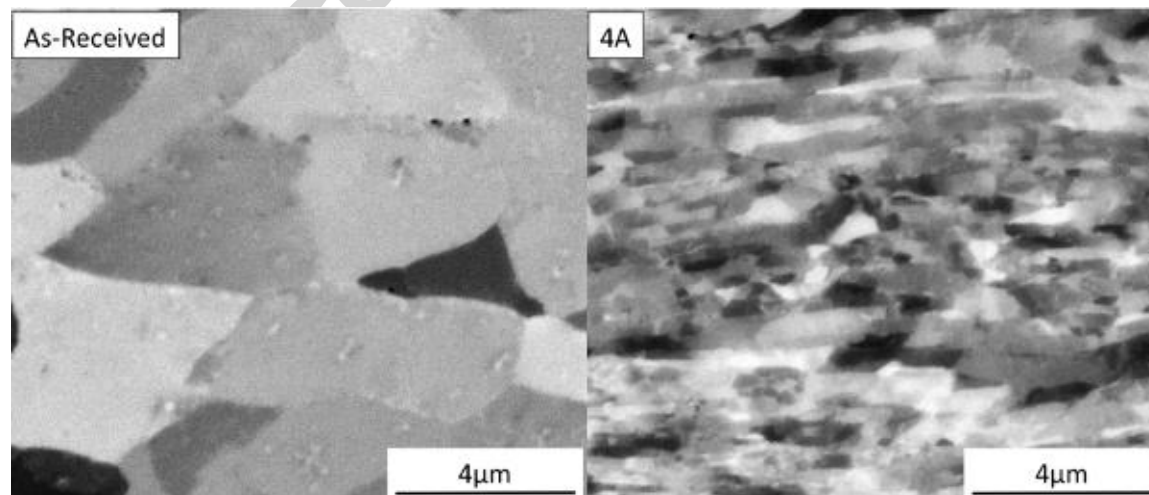


Figure 1: SEM – BSE images showing the microstructure of the as-received polycrystalline tungsten (left) and ECAE processed (4A) polycrystalline tungsten (right).

### 3.1 Three-point bend test

Optical images of the side view of the deformed specimens of the as-received and 4A materials tested under three-point bending at various test temperatures are shown in Fig. 2. The images of the deformed specimens were taken at the point of fracture or when the limit of the test apparatus has been reached. In the optical images, the highly deformed regions at the bend appear brighter than the surrounding material. The change in contrast is caused by the inelastic deformation induced changes in the surface topography that results in an increase in the reflected light. As seen in Fig. 2, the as-received material tested at temperatures below 150°C until the ambient temperature (24°C) do not show any inelastic deformation. Since no change in deformation mechanism is expected with further decrease in test temperature, no testing was done below ambient temperature. But, at test temperatures above 150°C, the as-received material exhibits significant inelastic deformation. At 300°C and above, the as-received material is sufficiently ductile to avoid fracture within the limits of the test apparatus where the maximum strain in the outer (bottom) portion of the specimen is nearly 40%. On the other hand, the 4A material exhibits inelastic deformation even at test temperatures as low as -45°C. But, the extent of inelastic deformation of the 4A material before fracture reaches a maximum for test temperatures slightly greater than 200°C and decreases thereafter. At ambient temperature, the strain at failure for the 4A material is ~20%.

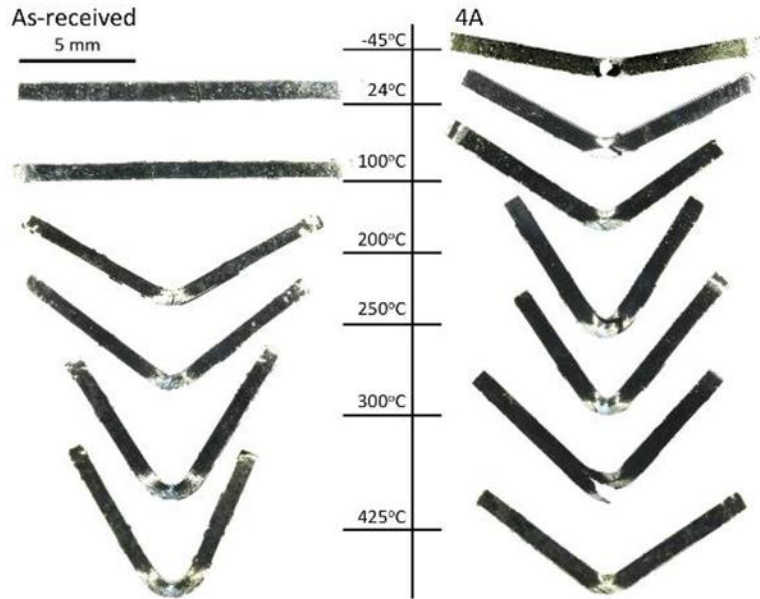


Figure 2: Optical images of the side view of the deformed three-point bend specimens of as-received and ECAE processed (4A) polycrystalline tungsten at various test temperatures.

The flexural stress-strain curves of the as-received and 4A materials for six test temperatures are shown in Fig. 3. The flexural stress  $\sigma_f$  and strain  $\varepsilon_f$  are estimated from the experimentally measured load-displacement data and initial specimen geometry following the relations;

$$\sigma_f = \frac{3FL}{2bd^2} \quad (1)$$

$$\varepsilon_f = \frac{6\delta d}{l} \quad (2)$$

Where  $F$  is the applied load,  $\delta$  is the applied displacement,  $l$  is the length of the specimen,  $b$  is the specimen width, and  $d$  is the specimen depth. As shown in Fig. 3(a), the as-received material exhibits a brittle response at low test temperatures and undergoes a brittle-to-ductile transition with increasing test temperatures. The brittle-to-ductile transition in the as-received material is marked by a decrease in the flexural stress at the onset of inelastic deformation and increase in the extent of inelastic deformation with increasing test temperature. On the contrary, the 4A material exhibits a ductile response at all test temperatures, as shown in Fig. 3(b). The flexural stress-strain response of the 4A material is also marked by a decrease in the flexural stress at the onset of inelastic deformation with increasing test temperature. But unlike the as-received material, the extent of inelastic deformation in the 4A material first increases with increasing test temperature and then tends to decrease for test temperatures (approximately) greater than  $\sim 200^\circ\text{C}$ . The flexural stress at the onset of inelastic deformation for the 4A material is greater than the as-received material at all the test temperatures. The inelastic deformation regimes of both the as-received and the 4A material, exhibit a brief period of strain hardening where the flexural stress increases with increasing flexural strain. Following the strain hardening regime for both the materials, the flexural stress gradually decreases with increasing flexural strain until final failure. For test temperatures less than  $\sim 200^\circ\text{C}$ , both the strain at the maximum flexural stress and the strain at failure for the 4A material is greater than the as-received material. This shows that the 4A material at these temperatures is not only more ductile but is more damage tolerant compared to the as-received material. For the test temperature of  $\sim 205^\circ\text{C}$ , the strain at the maximum flexural stress is comparable for both the 4A material and the as-received material, but the strain at failure for the 4A material is much greater than the as-received material. For higher test temperatures ( $>205^\circ\text{C}$ ) both the strain at the maximum flexural stress and the strain at failure for the as-received material is greater than those of the 4A material.

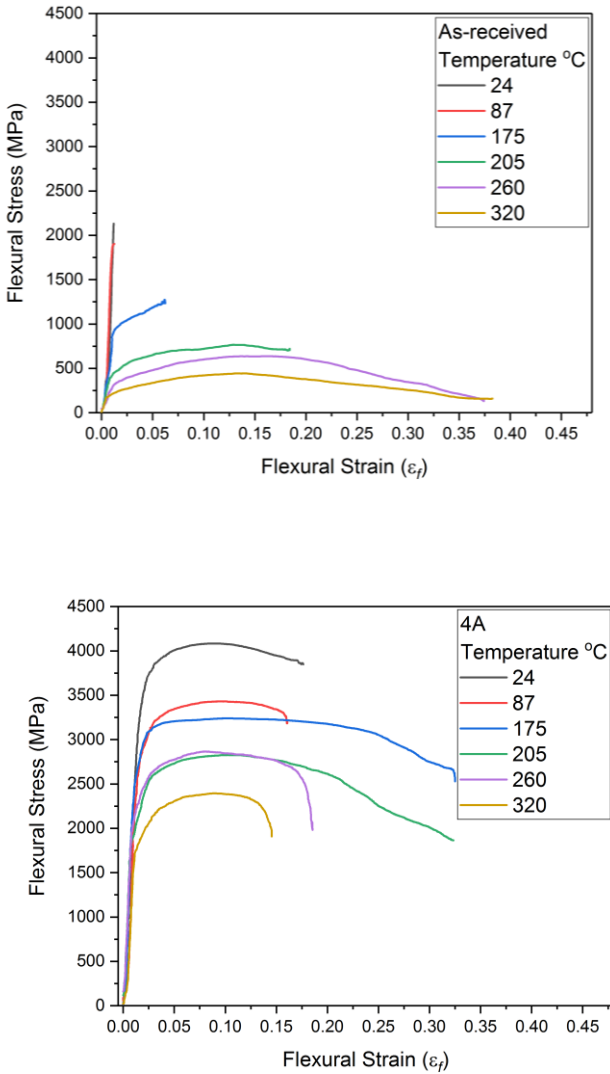


Figure 3: Flexural stress-strain curves of (a) the as-received and (b) the ECAE processed (4A) polycrystalline tungsten at various test temperatures.

### 3.2 Flexural toughness and brittle-to-ductile transition

The flexural toughness,  $(E_f)$ , is determined by integrating the load-displacement curve and normalizing it to the average initial cross-sectional area of the specimen for each test as described in Eq. (3). The cross-sectional area is used instead of the total volume of the specimen because the deformed volume was not constant between test specimens with different processing conditions. Thus, the flexural toughness defined by Eq. (3) quantifies the energy absorbed per unit cross-sectional area before fracture of a specimen without an initially dominant geometrical flaw. This, we believe, provides a better quantity than the specimen volume between bend supports for assessing the microstructural and temperature influence on bend fracture of the tested materials.



$$E_f = \frac{1}{bd} \int_{\delta_0}^{\delta} F d\delta \quad (3)$$

The variations in the flexural toughness with test temperature for the as-received material and three ECAE processed materials are shown in Fig. 4. The open symbols in the as-received data plot indicate specimens that did not fracture. A log scale is used for the vertical axis in Fig. 4 for better visualization because the toughness values for AR, 1A and 2A materials at low temperatures are orders of magnitude smaller than the 4A material. The values of the flexural toughness for the four materials over five temperature ranges are also summarized in Table 1.

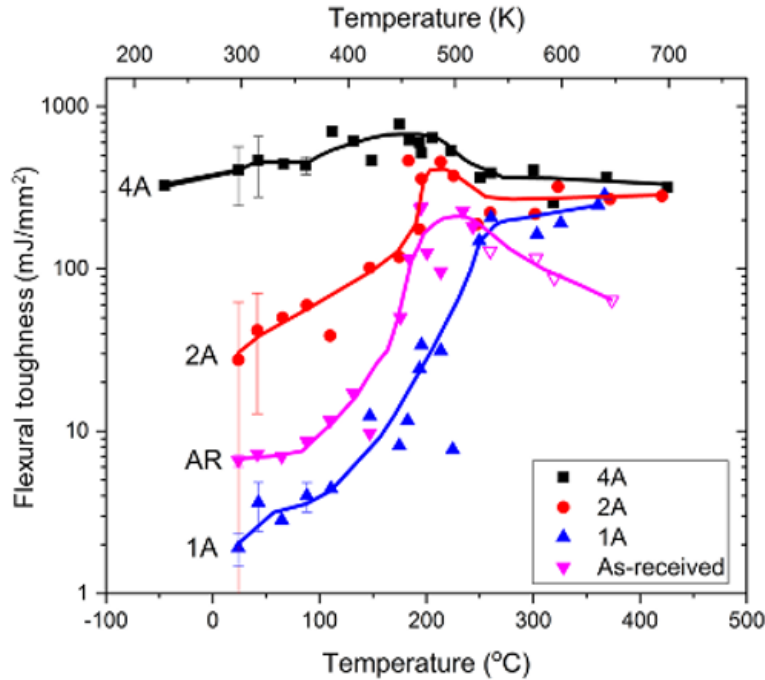


Figure 4: Variation in the flexural toughness with test temperature for as-received and ECAE processed (1A, 2A and 4A) polycrystalline tungsten.

Table 1: Average flexural toughness ( $\text{mJ/mm}^2$ ) obtained from three-point bend tests of as-received (AR) annealed and ECAE processed (1A, 2A and 4A) polycrystalline tungsten over select temperature ranges.

	Temperature ( $^{\circ}\text{C}$ )					
Processing	24	24-100	100-150	150-200	200-300	>300
AR	$6.6 \pm 0.6$	$8 \pm 1$	$13 \pm 4$	$160 \pm 94$	$150 \pm 52$	$90 \pm 26$
1A	$1.9 \pm 0.4$	$3.5 \pm 0.6$	$8 \pm 6$	$20 \pm 12$	$100 \pm 95$	$220 \pm 55$
2A	$27 \pm 35$	$50 \pm 21$	$70 \pm 44$	$280 \pm 160$	$310 \pm 125$	$272 \pm 42$
4A	$400 \pm 160$	$448 \pm 115$	$594 \pm 120$	$629 \pm 110$	$481 \pm 115$	$336 \pm 65$

As shown in Fig. 4, the flexural toughness of the as-received material increases rapidly from  $6 \text{ mJ/mm}^2$  at ambient temperature to  $240 \text{ mJ/mm}^2$  near  $200^{\circ}\text{C}$ , and then it decreases to  $64 \text{ mJ/mm}^2$  at  $370^{\circ}\text{C}$ . This behavior is consistent with observations in other polycrystalline tungsten rods

showing a maximum in toughness at similar temperatures [18]. The observed variation in toughness with test temperature for the 1A material is also similar to the observation of Rupp and Weygand, where they observed a shift in brittle-to-ductile transition with prior deformation towards higher temperatures [5]. Due to this shift, the 1A material does not appear to have reached peak toughness within the temperature range explored here. From Fig. 4, the toughness of the 1A material seems to be greater than that of the as-received material for temperatures greater than  $\sim 250^{\circ}\text{C}$ . But it should be noted that the as-received material did not fracture catastrophically at these elevated temperatures and continued to undergo inelastic deformation. Unlike the single-extrusion 1A material, additional ECAE passes resulted in a substantial increase in ambient temperature toughness for both 2A and 4A processed tungsten. At ambient temperature the 2A material has a toughness of  $27.5\text{mJ/mm}^2$ , whereas the toughness of 4A material exceeds  $405\text{mJ/mm}^2$ , resulting in approximately 4 and 67 times increases in ambient temperature toughness compared to the 2A and as-received materials, respectively. However, similar to the as-received material, the toughness of both 2A and 4A material peaks at a temperature near  $200^{\circ}\text{C}$ , with maximums in toughness of  $455\text{mJ/mm}^2$  and  $780\text{mJ/mm}^2$  for the 2A and 4A materials, respectively.

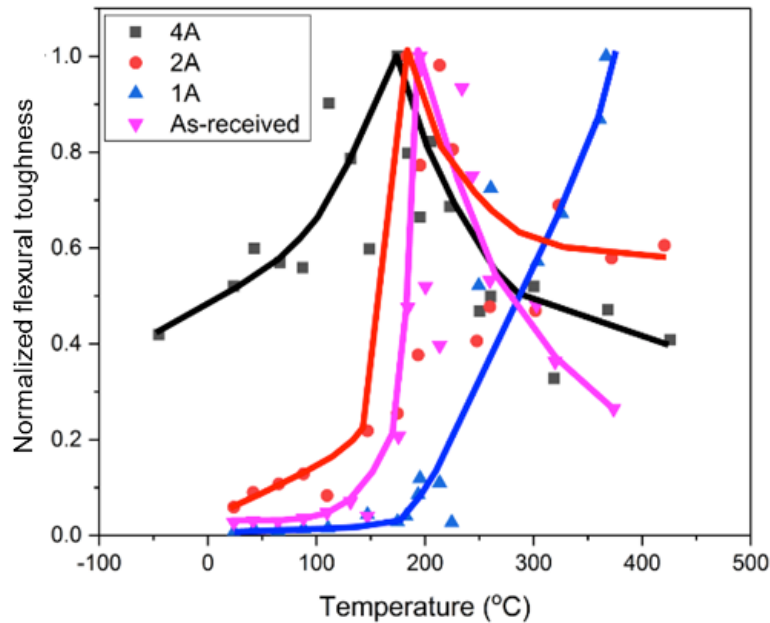


Figure 5: Variation in the flexural toughness normalized to the maximum flexural toughness of the material with test temperature for as-received and ECAE processed (1A, 2A and 4A) polycrystalline tungsten.

Figure 5 shows the variation in the normalized flexural toughness with test temperature. The flexural toughness normalized with the maximum flexural toughness provides a better estimate of the location of the peak fracture toughness on the temperature scale compared to flexural toughness alone (Fig. 4). We use the location of the peak in flexural toughness to determine the brittle-to-ductile transition temperature instead of assigning a threshold toughness value. The rationales behind adopting this procedure are: (i) this method is analogous to that used previously for single crystal tungsten [3] except for replacing fracture toughness with flexural toughness, and (ii) the significant ductility observed in the 4A material would provide a false indication of

the brittle-to-ductile transition relative to as-received and other ECAE processed materials. As shown in Fig. 5, the maximum toughness for the as-received, 2A and 4A materials correspond to approximately 195°C, 183°C and 175°C, respectively. We acknowledge that this decrease in transition temperature can be lost because of simple statistical error. Note that the maximum toughness for the 1A material is not observed within the range of temperatures tested. In addition, the normalized toughness of both as-received and 2A materials decrease rapidly with temperature below ~200°C. However, the 4A material shows a rather gradual decrease in normalized toughness with temperature below ~200°C.

### 3.3 Failure analysis

To better understand the microstructural and thermal influence on bend fracture of tungsten, a comprehensive failure analysis of all the specimens was carried out. Representative fracture surfaces of as-received and the three ECAE processed polycrystalline tungsten specimens tested at ambient temperature are shown in Fig. 6. The as-received material failed predominantly by intergranular separation of the sub-grain boundaries with limited instances of transgranular fracture. The fracture surface of the as-received material shown in Fig. 6(a), shows features of both intergranular and smooth facets of comparatively rare transgranular fracture (marked by arrow for the purpose of demonstration). Following one ECAE pass (1A), fracture is dominated by transgranular cleavage, with some intergranular separation as shown in Fig. 6(b). The intergranular separation, indicated by arrows in Fig. 6(b), appears as a stepped surface along the fracture path. The transgranular cleavage mode of fracture is also a dominant fracture mode in 2A material, but the fracture path appears more tortuous than in the 1A material. Radiating planar surfaces near the center of Fig. 6(c) indicate some inelastic deformation prior to failure. Few instances of intergranular separation are also visible in Fig. 6(c) as indicated by the arrow. But these intergranular separations in the 2A material do not have the horizontal step-like character observed in the 1A material. Unlike the other two ECAE processed materials (1A and 2A), the fracture surface of the 4A tungsten shown in Fig. 6(d) is remarkably distinct. Fracture in the 4A material seems analogous to that in a laminated composite, with continuous intergranular separation and transgranular fracture.

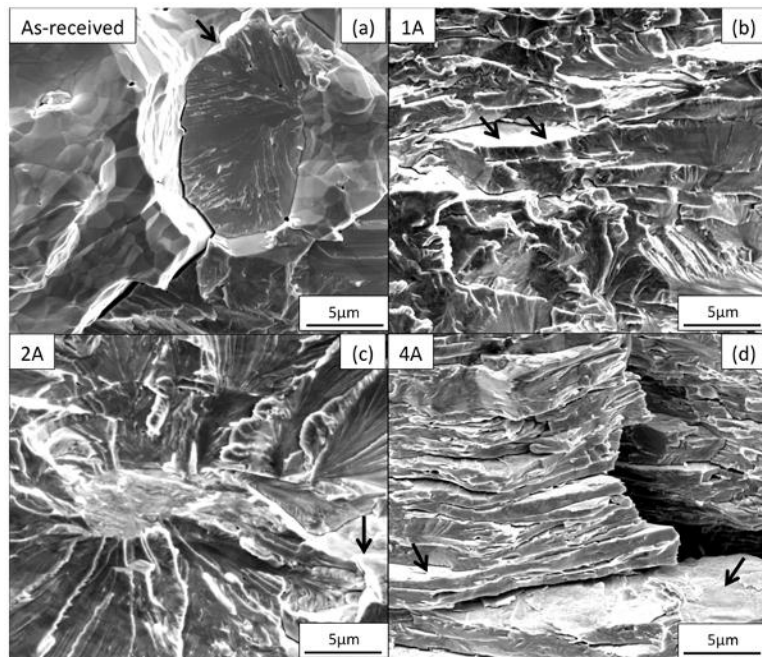


Figure 6: SEM – SE images of the fracture surfaces of the tungsten specimens tested under three-point bending at 24°C: (a) as-received, (b) 1A, (c) 2A, and (d) 4A specimens. Arrows indicate a transgranular fracture region in (a) as-received, and intergranular fracture regions in ECAE processed materials (b-d).

The SEM images of the side-view of a fractured specimen of the as-received material tested at 24°C are shown in Fig. 7. At ambient temperature no macroscopic inelastic deformation is seen in the as-received materials prior to fracture. As shown in Fig. 7(a), the macroscopic crack path is not entirely parallel to the applied loading direction causing bending. The crack propagation mode in this material is predominantly intergranular and the zoomed-in view of the region marked by a dashed rectangle in Fig. 7(a), shown in Fig. 7(b), captures an instance of crack branching at a grain boundary junction. In Fig. 7(b) intergranular separation along both the grain and subgrain boundaries can be seen, with the primary crack circumventing the subgrains. It is assumed that these features are subgrains based on the lack of etching observed during polishing as opposed to more susceptible grain boundaries that preferentially etch. Further investigation of the highlighted region in Fig. 7(b), illustrates fracture by intergranular separation of subgrains, as well as some transgranular cleavage. The zoomed-in view of the secondary crack tip highlighted in Fig. 7(c) is shown in Fig. 7(d). The secondary crack in Fig. 7(d) is arrested within a tungsten grain and significant strain contrast surrounding this crack tip is noted. This provides qualitative evidence behind the idea of excessive resistance to transgranular cleavage in the as-received material.

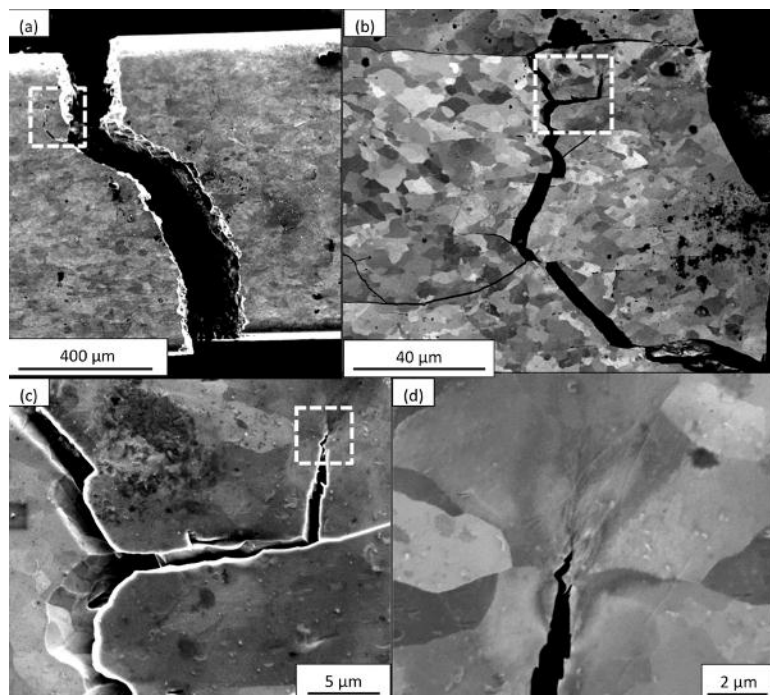


Figure 7: SEM images of the side view of an as-received tungsten specimen tested until fracture under three-point bending at 24°C. The images in (a) and (c) are SEM-SE images, while (b) and (d) are SEM-BSE images. The zoomed-in views of the areas inscribed by dashed white rectangles are shown in the subsequent images.

Figure 8 shows the SEM images of the side-view of a fractured specimen of 4A processed tungsten tested at 24°C. The 4A specimen underwent a large amount of inelastic deformation prior to fracture at ambient temperature as evident from Figs. 2, 3 and 8(a). Unlike the as-received material, the crack path in 4A material is highly tortuous with long secondary and occasional tertiary cracks. The short secondary cracks are often very similar to the primary crack involving continuous intergranular separation and transgranular fracture whereas the long secondary cracks are predominantly due to a delamination type failure along tungsten lamellae most likely separated by original grain boundaries. Figure 8(b) marks two cracks: the bottom one is a long crack originating from delamination of tungsten lamella whereas the crack running across the image is due to continuous intergranular separation and transgranular fracture. A higher magnification view of the secondary crack due to continuous intergranular separation and transgranular fracture is shown in Fig. 8(c), and a zoomed-in view of a long secondary crack due to delamination of tungsten lamella is shown in Fig. 8(d). The superposition of the two crack growth modes, continuous intergranular separation – transgranular fracture, and delamination of tungsten lamellae, causes the primary crack to deflect at  $\sim 45^\circ$  from the applied loading direction caused by bending.

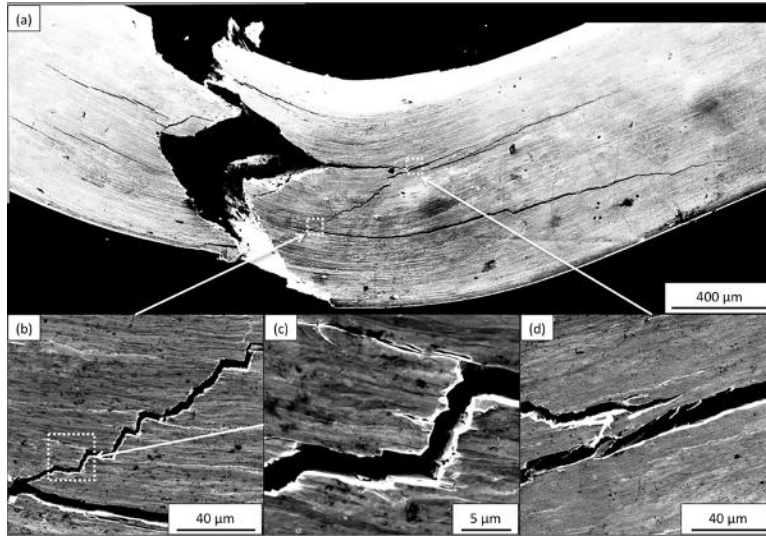


Figure 8: SEM images of the side view of a 4A processed tungsten specimen tested until fracture under three-point bending at 24°C. The images in (a), (b) and (d) are SEM-SE images, while (c) is an SEM-BSE image.

In order to further investigate the initiation of failure in the 4A material, a sample of 4A material was deformed to approximately 90% of failure in three-point bending. The SEM image of the side view of this unbroken test specimen is shown in Fig. 9(a), with zoomed-in views of the regions under compression and tension shown in Figs. 9(b) and (c). The formation of shear bands and local buckling of lamella together with inter-lamella decohesion in the compressive region of the specimen can be seen in Fig. 9(b). The formation of shear bands is visible in the tensile region, Fig. 9(c). Additionally, in Fig. 9(c) three types of micro-cracks can be seen. Proceeding from longest to shortest, these micro-cracks are: (i) inter lamella cracks along the extrusion direction; (ii) intergranular cracks along the grain boundaries parallel to the applied loading direction; and (iii) sharp cracks within the tungsten lamella.

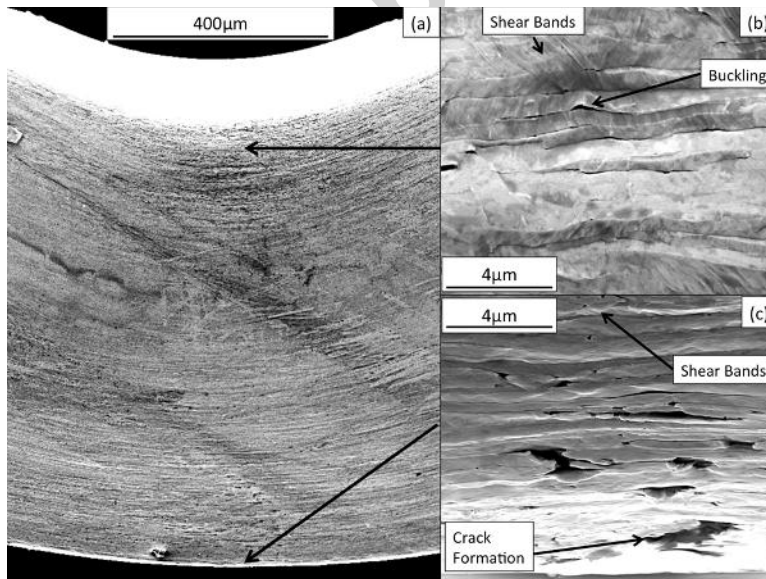


Figure 9: SEM-SE images of the side view of a 4A processed tungsten specimen deformed to 90% of the expected fracture deflection under three-point bending at 24°C.

Side-view SEM images of a fractured as-received material specimen tested at 210°C are shown in Fig. 10. The curvature of the specimen seen in Fig. 10(a) indicates a significant amount of inelastic deformation prior to fracture. Evidence of severe deformation can also be seen towards the bottom of the specimen in Fig. 10(a) due to roughening (orange peel effect) of the surface. As shown in Fig. 10(a), the deviation of the macroscopic crack path from the applied loading direction causing bending is significantly less at 210°C compared to ambient temperature, Fig. 7(a). This indicates a transition to the transgranular fracture mode in the as-received material with increasing test temperature. The transgranular fracture mode can be seen in the magnified image of the crack path in Fig. 10(b). Extensive shear bands and secondary cracks correlate with an increase in ductility with increasing temperature.

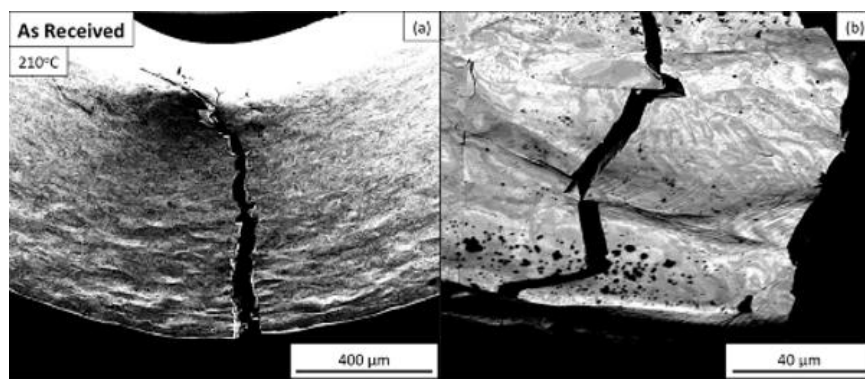


Figure 10: SEM images of the side view of an as-received tungsten specimen tested until fracture under three-point bending at 210°C. The image in (a) is an SEM-SE image, while that in (b) is an SEM-BSE image.

Figure 11 shows the side view of a fractured specimen of 4A processed tungsten tested at 360°C. Fracture at this temperature appears to be primarily due to a combination of inter lamella delamination and transgranular fracture. This fracture mode results in significant crack deflection from the applied loading direction. The transgranular fracture is preceded by significant inelastic deformation in the elongated tungsten grains, as seen in Fig. 11(b). However, unlike the ambient temperature case (Fig. 8), here there is an absence of secondary cracks through delamination that alternate in direction across the sample.



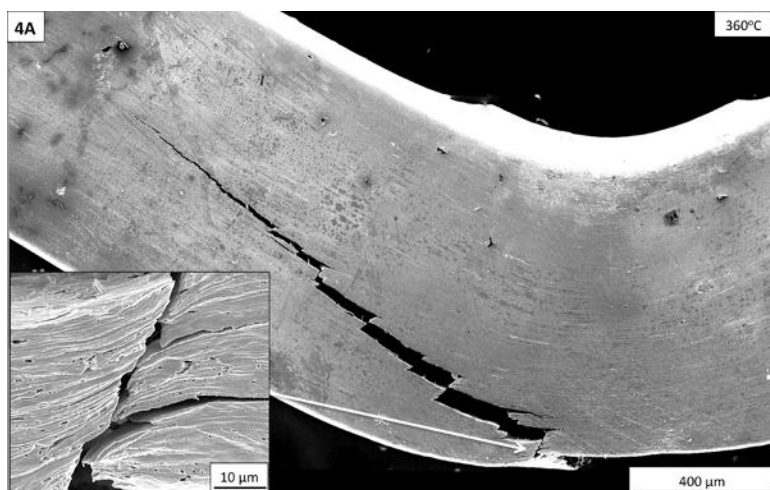


Figure 11: SEM-SE images of the side view of a 4A processed tungsten specimen tested until fracture under three-point bending at 360°C. The zoomed-in view of the region marked by the arrow is shown in the inset.

The overall crack deflection angles for as-received and 4A materials are summarized in Fig. 12. Error bars in the figure indicate the standard deviation of repeated deflection angle measurements made on different specimens. The crack deflection angle for the as-received material at 24°C exceeds 30°, and decreases linearly to less than 10° at the ~250°C test temperature. This clearly shows the change in fracture mode from intergranular to transgranular with increasing temperature in the as-received material. For temperatures greater than 250°C the as-received material did not undergo catastrophic fracture.

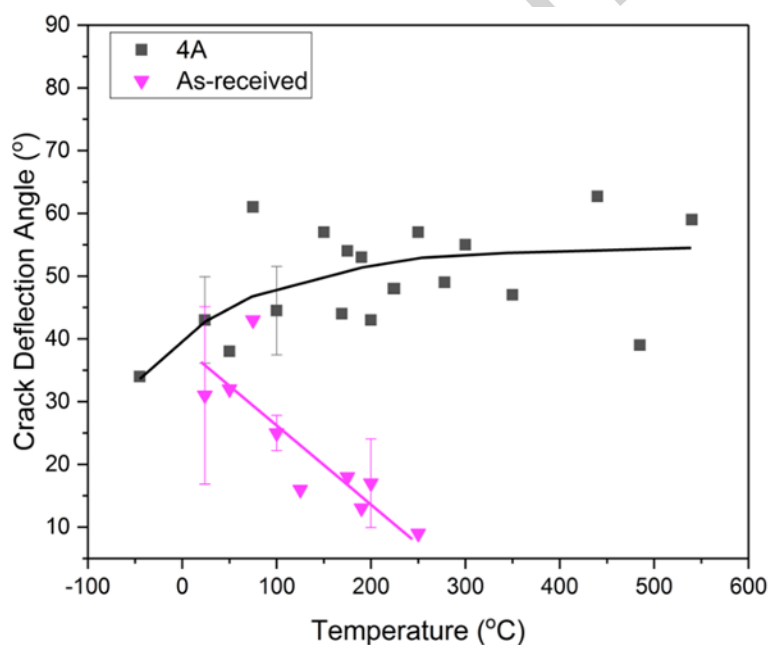


Figure 12: Variation of crack deflection angle with test temperature for as-received and 4A processed polycrystalline tungsten under three-point bending.



On the other hand, the crack deflection angle for the 4A material is  $\sim 35^\circ$  at  $-45^\circ\text{C}$  and increases with increasing test temperature to nearly  $50^\circ$  at  $200^\circ\text{C}$ . Above  $200^\circ\text{C}$  the extent of crack deflection on an average stays constant for the 4A material. This clearly shows that the 4A processed material undergoes fracture via continuous intergranular separation and transgranular fracture at all temperatures. But the extent of transgranular separation increases with increasing temperature until  $\sim 200^\circ\text{C}$  (transition temperature) and thereafter stays constant.

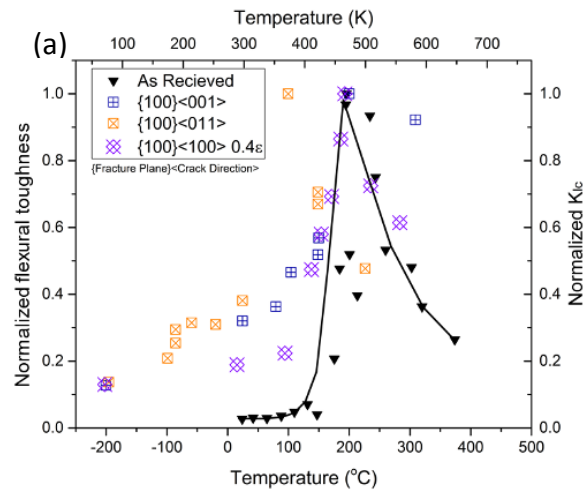
#### 4. Discussion

The brittle-to-ductile transition in the as-received (unprocessed) tungsten is typical of polycrystalline tungsten, as has been reported in [19]. The shift in the brittle-to-ductile transition towards a higher temperature in the 1A processed material is also in line with previous observations in both pre-deformed single crystal [3] and polycrystalline [20] tungsten. This shift in the transition temperature with pre-deformation is in general attributed to the pinning of preexisting dislocations, resulting in decreased ductility. However, the presence of a greater dislocation density cannot explain the brittle-to-ductile transition behavior of the more heavily deformed, the 2A and 4A processed materials, for which the transition temperature is slightly lower than (or the same as) the transition temperature of the as-received material as indicated in Fig. 5.

In Fig. 13, we compare the variation in the normalized flexural toughness with test temperature of the as-received and the 4A processed materials obtained in this work, along with the variation in the normalized fracture toughness of single crystal tungsten with test temperatures reported in [2, 3]. The normalized quantities are obtained by dividing each of the values with the respective maximum value. We note that the two quantities, flexural toughness of polycrystalline tungsten and fracture toughness of single crystal tungsten, being compared in Fig. 13, are not directly related. Transgranular fracture of a polycrystalline material is much more complicated than fracture of single crystals because of the presence of grain boundaries, orientation distribution of grains, and constraint imposed by the neighboring grains in polycrystalline material. However, the variation in the normalized fracture toughness of single crystal tungsten with test temperature indicates the ease of activation of a particular crack system with test temperature. Thus, a comparison of the temperature dependent variation in the normalized flexural toughness of the as-received and the 4A processed materials, with the temperature dependent variation in the normalized fracture toughness of single crystal tungsten offers some insight into the preferred crack system for transgranular fracture in the polycrystalline material at a given test temperature. In [2, 3], the fracture toughness of single crystals was measured in the  $\langle 001 \rangle$  or  $\langle 011 \rangle$  direction on  $\{100\}$  and  $\{110\}$  planes. These combinations of the crack plane and crack direction make up the families of the preferred crack systems in tungsten crystals. As shown in Fig. 13, the normalized toughness peak of both materials roughly coincides with the temperature at which the peaks in the normalized fracture toughness of the single crystals are observed. Also, the similarities between the dependence of normalized toughness on temperature for the as-received material and the  $\{100\}$  systems and the 4A processed material and the  $\{110\}$  systems are noted from Figs. 13(a) and (d), respectively. The only difference is that the normalized toughness of the as-received material is nearly constant up to  $100^\circ\text{C}$  whereas the normalized fracture toughness of the single crystals with the  $\{100\}$  crack systems increases steadily up to  $100^\circ\text{C}$ , Fig.

13(a). But, for temperatures greater than 100°C, both the normalized toughness of the as-received material, and the normalized fracture toughness of the single crystals with {100} crack systems, increases nearly exponentially up to the transition temperature.

The difference between the as-received material and single crystals with {100} crack systems for temperatures approximately less than 100°C is probably due to the fact that the as-received polycrystalline tungsten at low temperatures preferentially undergoes intergranular fracture, Fig. 7. The similarity between the as-received material and single crystals with {100} crack systems for temperatures greater than 100°C is due to the fact that at high temperatures the as-received material predominantly undergoes transgranular fracture as seen in Fig. 10. For transgranular fracture in untextured materials, it can be assumed that fracture occurs along {100} crack systems because these systems, the {100}  $\langle 001 \rangle$  and  $\langle 011 \rangle$ , have the lowest fracture toughness and would thus fracture preferentially. The 4A material, on the other hand, has a lamellar microstructure with strong {110} and {111} texture along the extrusion direction (i.e. the tensile loading direction under three-point bending) so that transgranular fracture in these materials preferentially occurs along the {110} family of crack systems. Also, the grain boundaries in the 4A processed material are significantly strengthened by the prior plastic deformation during ECAE processing so that intergranular fracture can be assumed to be less sensitive to changes in temperature. These descriptions provide a rationale for the similarity between the 4A material and single crystals with {110} crack systems.



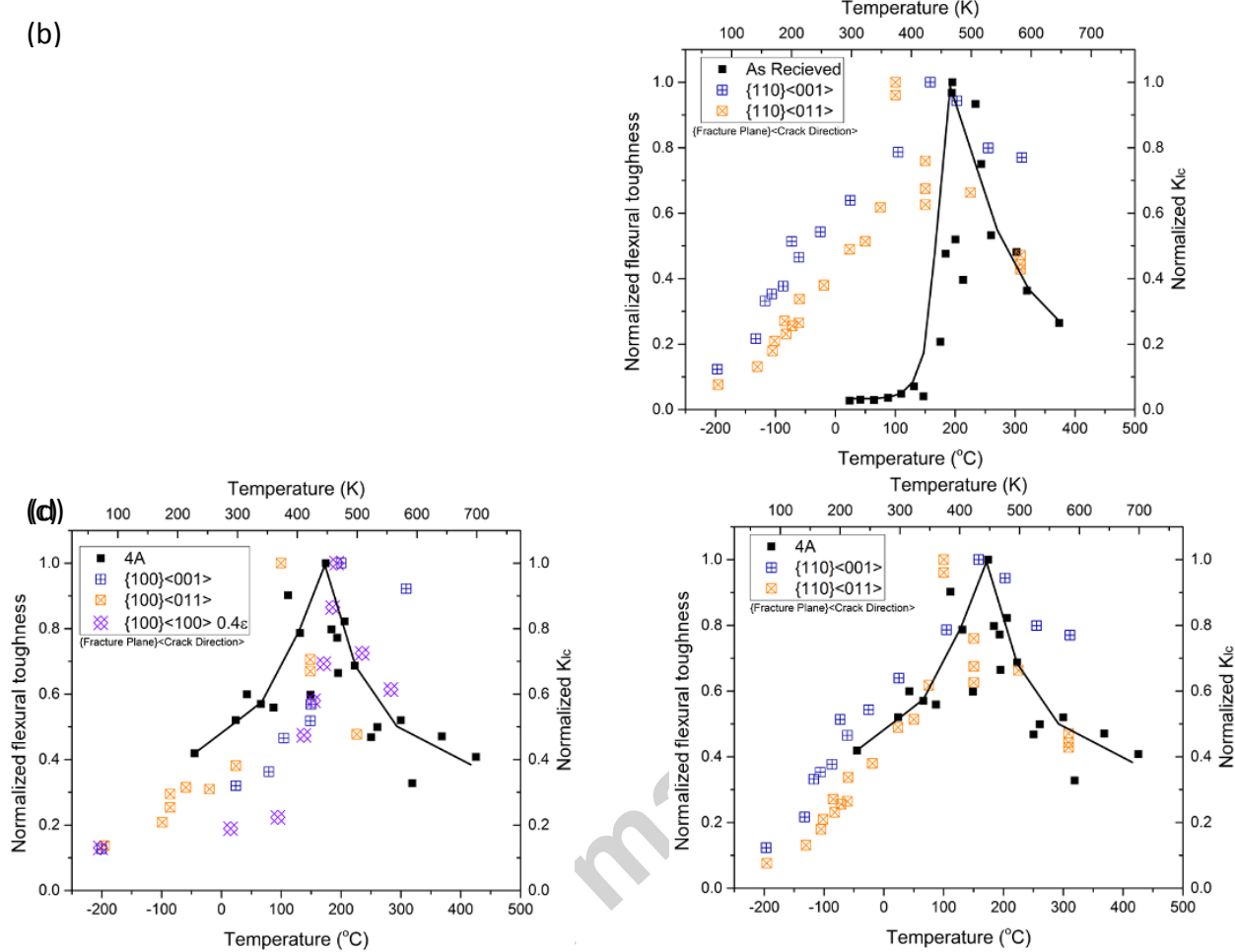


Figure 13: Comparison of the temperature dependent normalized flexural toughness data (filled square symbols) from this study, and normalized fracture toughness data from single crystal experiments [2, 3]. (a) As-received material compared with {100} family of crack systems. (b) As-received material compared with {110} family of crack systems. (c) 4A processed material compared with {100} family of crack systems. (d) 4A processed material compared with {110} family of crack systems. All data are normalized by the maximum value for each data set.

The fact that the ductility and flexural toughness of the 4A processed material is significantly greater than that of the as-received material at temperatures lower than the brittle-to-ductile transition temperature, Figs. 3 and 4, is noteworthy. This behavior is probably due to several complementary effects. The 4A processed material has a lamellar microstructure with elongated grains. Elongation of the grains due to severe plastic deformation improves the grain-to-grain bonding by physically creating new and clean boundaries [21]. In addition, the increase in grain boundary area dilutes the interstitial impurities at the boundaries. This will enhance the resistance to intergranular fracture. The fracture mechanism of 4A material involves continuous intergranular separation and transgranular fracture at all temperatures. This also results in significant crack deflection compared to as-received material, Fig. 12. Thus, in the 4A processed material the greater low temperature ductility and toughness is in part due to the microstructural changes that inhibit the formation of cracks and enhances crack growth resistance. This in turn

results in a significant increase in the stress level in the material needed for fracture. A sufficient increase in the stress level can then possibly free up pinned dislocations resulting in plastic deformation. Additionally, the strong {110} and {111} texture along the extrusion direction enables activation of the relatively high fracture toughness {110}  $\langle 001 \rangle$  and/or  $\langle 011 \rangle$  crack systems for transgranular fracture.

## 5. Summary and Conclusions

Bulk polycrystalline tungsten with annealed and severally deformed microstructures were tested under three-point bending over a range of temperature above and below the brittle-to-ductile transition temperature. The flexural stress, maximum tensile strain at failure, and toughness were measured, and crack initiation and propagation phenomena characterized. Several trends were observed and compared with single-crystal and polycrystalline tungsten studies available in the literature. The key findings and conclusions of this work are:

At ambient temperature:

1. Fracture in annealed tungsten under three-point bending is dominated by intergranular cracking, while pre-deformed microstructures fail by a combination of intergranular and transgranular cracking. The extent and length of intergranular cracking increases with increasing prior workpiece deformation/grain elongation.
2. Prior to failure in the most heavily pre-deformed material (strains exceeding 4.5), shear bands are observed along with the formation of inter lamella micro-cracks. These inter lamella micro-cracks grow with increased bending along the axis of the bend specimen, resulting in an increase in flexural stress. The final failure occurs by continuous intergranular separation and transgranular fracture.
3. The most heavily pre-deformed bulk pure tungsten exhibits a greater than 50 times increase in flexural toughness compared to annealed pure polycrystalline tungsten. This is due to the microstructural changes that increase the resistance to intergranular crack nucleation and growth. This in turn increases the stress level in the material that can free up pinned dislocations resulting in increased plastic dissipation. Additionally, the texture along the extrusion direction enables activation of the relatively high fracture toughness crack systems for transgranular fracture.

Influence of test temperature:

4. In the annealed material the extent of crack deflection away from the applied loading direction causing bending decreases with increasing temperature until the brittle-to-ductile transition temperature is reached. This reflects a transition from intergranular to transgranular fracture with increasing temperature.
5. In the most heavily pre-deformed material, fracture occurs by continuous intergranular separation and transgranular fracture at all temperatures so that the extent of crack deflection away from the applied loading direction remains high for the range of test temperature considered.
6. The flexural toughness of the most heavily pre-deformed material is greater than that of the annealed material at all temperatures. This is at least in part due to the microstructural

changes that increases the resistance to intergranular fracture, enhances plastic dissipation, and activates relatively high fracture toughness crack systems for transgranular fracture.

7. The variation in the normalized toughness of the bulk polycrystalline tungsten especially that of the most heavily pre-deformed material, with test temperature is very similar to that of the single crystal tungsten. This is probably due to the fact that the grain boundaries of the heavily pre-deformed material are significantly strengthened so that intergranular fracture in these materials is less sensitive to changes in temperature, while the strong texture preferentially activates the transgranular crack systems similar to the case of single crystals.
8. The brittle-to-ductile transition temperature of the pure tungsten increases slightly after moderate prior deformation, but heavily pre-deformed and annealed materials share a similar transition temperature.

## Acknowledgements

The authors thank the efforts of Robert Barber for his assistance with material processing. The facilities at Texas A&M University and financial support from ARMY contract W15QKN15C0031 to Shear Form, Inc., and the US Air Force SMART scholarship program, are gratefully acknowledged.

## References

1. Jeffries, Z., *Metallography of Tungsten*. Transactions of the American Institute of Mining and Metallurgical Engineers, 1919. **60**: p. 588-643.
2. Gumbsch, P., J. Riedle, A. Hartmaier, and H.F. Fischmeister, *Controlling Factors for the Brittle-to-Ductile Transition in Tungsten Single Crystals*. Science, 1998. **282**(5392): p. 1293-1295.
3. Gumbsch, P., *Brittle Fracture and the Brittle-to-Ductile Transition of Tungsten*. Journal of Nuclear Materials, 2003. **323**(2-3): p. 304-312.
4. Rupp, D. and S.M. Weygand, *Experimental Investigation of the Fracture Toughness of Polycrystalline Tungsten in the Brittle and Semi-Brittle Regime*. Journal of Nuclear Materials, 2009. **386**: p. 591-593.
5. Rupp, D. and S. Weygand, *Anisotropic Fracture Behaviour and Brittle-to-Ductile Transition of Polycrystalline Tungsten*. Philosophical Magazine, 2010. **90**(30): p. 4055-4069.
6. Habainy, J., S. Iyengar, Y. Lee, and Y. Dai, *Fatigue Behavior of Rolled and Forged Tungsten at 25°, 280° and 480° C*. Journal of Nuclear Materials, 2015. **465**: p. 438-447.
7. Stephens, J.R., *Effects of Interstitial Impurities on the Low-Temperature Tensile Properties of Tungsten*, 1964, DTIC Document.
8. Pan, Z., L.J. Kecskes, and Q. Wei, *The Nature Behind the Preferentially Embrittling Effect of Impurities on the Ductility of Tungsten*. Computational Materials Science, 2014. **93**: p. 104-111.
9. Krasko, G.L., *Effect of Impurities on the Electronic Structure of Grain Boundaries and Intergranular Cohesion in Iron and Tungsten*. Materials Science and Engineering a-Structural Materials Properties Microstructure and Processing, 1997. **234**: p. 1071-1074.
10. Allen, B.C., D.J. Mayhuth, and R.I. Jaffee, *The Recrystallization and Ductile-Brittle Transition Behaviour of Tungsten-Effect of Impurities on Polycrystals Prepared from Single Crystals*. Journal of Institute of Metals, 1961. **90**(4): p. 120-128.

11. Margevicius, R.W., J. Riedle, and P. Gumbsch, *Fracture Toughness of Polycrystalline Tungsten under Mode I and Mixed Mode I/II Loading*. Materials Science and Engineering: A, 1999. **270**(2): p. 197-209.
12. Lee, H. and V. Tomar, *Understanding Effect of Grain Boundaries in the Fracture Behavior of Polycrystalline Tungsten under Mode-I Loading*. Journal of Engineering Materials and Technology-Transactions of the Asme, 2012. **134**(3).
13. Schade, P., *Wire Drawing Failures and Tungsten Fracture Phenomena*. International Journal of Refractory Metals and Hard Materials, 2006. **24**(4): p. 332-337.
14. Funkenbusch, A., F. Bacon, and D. Lee, *The Influence of Microstructure on Fracture of Drawn Tungsten Wire*. Metallurgical Transactions A, 1979. **10**(8): p. 1085-1091.
15. Leber, S., J. Tavernelli, D. White, and R. Hehemann, *Fracture Modes in Tungsten Wire*. Journal of the Less Common Metals, 1976. **48**(1): p. 119-133.
16. Segal, V., K. Hartwig, and R. Goforth, *In Situ Composites Processed by Simple Shear*. Materials Science and Engineering: A, 1997. **224**(1-2): p. 107-115.
17. Levin, Z. and K. Hartwig, *Strong Ductile Bulk Tungsten*. Materials Science and Engineering: A, 2017.
18. Rupp, D., R. Mönig, P. Gruber, and S. Weygand, *Fracture Toughness and Microstructural Characterization of Polycrystalline Rolled Tungsten*. International Journal of Refractory Metals and Hard Materials, 2010. **28**(6): p. 669-673.
19. Krsjak, V., S.H. Wei, S. Antusch, and Y. Dai, *Mechanical Properties of Tungsten in the Transition Temperature Range*. Journal of Nuclear Materials, 2014. **450**(1-3): p. 81-87.
20. Giannattasio, A., Z. Yao, E. Tarleton, and S.G. Roberts, *Brittle-Ductile Transitions in Polycrystalline Tungsten*. Philosophical Magazine, 2010. **90**(30): p. 3947-3959.
21. Segal, V.M., *Materials Processing by Simple Shear*. Materials Science and Engineering: A, 1995. **197**(2): p. 157-164.